ADVANCED ENERGY MATERIALS

www.MaterialsViews.com

ADVANCED
ENERGY
MATERIALS
www.advenergymat.de

COMMUNICATION

Doubling the Power Output of Bifacial Thin-Film GaAs Solar Cells by Embedding Them in Luminescent Waveguides

Xing Sheng, Ling Shen, Taehwan Kim, Lanfang Li, Xinran Wang, Ryan Dowdy, Paul Froeter, Kazuki Shigeta, Xiuling Li, Ralph G. Nuzzo, Noel C. Giebink,* and John A. Rogers*

Recent developments in epitaxial liftoff techniques for forming thin, high efficiency GaAs solar cells create opportunities to improve the economics of solar energy conversion by combining highly efficient operation with the prospect of scalable, low cost manufacturing, especially in advanced growth schemes that involve multiple layers in releasable stacks.[1,2] These cells require GaAs at thicknesses of just a few microns or less, and can offer efficiencies as high as 28.8%.[3] Efforts to reduce costs focus on techniques to improve the utilization of the growth chambers by accelerating the deposition rates and/ or by eliminating cycles of load/unload,[1] and on methods to reuse the growth wafers. Additional routes involve schemes for concentrating incident sunlight. In small-scale devices, focusing micro-optics can be used, to achieve concentration ratios greater than 1000× with levels of uniformity in illumination, and tolerance in acceptance angles that enable practical modules with a world record efficiency of 33.9%.[4] Luminescent solar concentrators (LSCs) could represent an alternative or complementary approach, with the potential to eliminate or reduce the need for tracking. Recent implementations provide enhanced properties, by use of distributed arrays of small cells that embed directly in the LSC, as initially reported with silicon devices.[5,6]

Thin-film GaAs microscale cells (μ-cells) that combine epitaxial liftoff from single or multilayer epitaxial assemblies and transfer printing to substrates of interest increase the range of engineering design options for these and related classes of photovoltaic materials.[1] Here, we show that such μ-cells can be used within LSCs to increase the power output by more than a factor of two, thereby providing a potentially important route to reducing costs while maintaining high efficiencies. An LSC consists of a planar waveguide doped with a luminescent dye designed to absorb incoming sunlight and then to emit into confined modes, for subsequent capture by attached solar cells.[7–14] LSCs operate independent of incident angle, in principle surpassing both the sine[15] and ergodic limits[16] due to the down-shift in photon energy.[17] The traditional LSC design incorporates solar cells attached to the waveguide edges;[14] in this geometry, the cells do not receive any direct sunlight and instead rely entirely on waveguided luminescence. In contrast, recently reported LSC systems that employ surface-embedded bifacial silicon μ-cells offer an inherent advantage in efficiency because each cell generates power both from direct illumination and waveguided luminescence.[6] More fundamentally, the capability to absorb light through both sides of the cell increases its occupation of optical phase space when embedded within an LSC, leading to an increased thermodynamic concentration limit as compared to a conventional LSC with edge-mounted cells.[18]

Figure 1 shows devices that involve GaAs solar μ-cells delivered onto LSC substrates using the techniques of transfer printing.[1,12] The cells use a GaAs based vertical junction (Figure 1b), with lateral dimensions of 240 μm by 200 μm. The thickness of the heavily doped n-GaAs bottom contact layer is thinned to 300 nm to improve the yield of photons collected from the backside. The μ-cells are released from the growth substrate by selective etching of a base layer of $Al_{0.95}Ga_{0.05}As$ with hydrofluoric acid. Transfer printing delivers the devices onto LSC substrates, as shown in Figure 1a. The LSC layer consists of an ultraviolet (UV) cured polymer (NOA61, Norland Products Inc.) doped with a luminescent DCM

Dr. X. Sheng, [†] Dr. L. Li, Dr. X. Wang, Dr. K. Shigeta,
Prof. J. A. Rogers
Department of Materials Science and Engineering
and Frederick Seitz Materials Research Laboratory
University of Illinois at Urbana-Champaign
Urbana, IL 61801, USA
E-mail: jrogers@illinois.edu
T. Kim, Prof. N. C. Giebink
Department of Electrical Engineering
The Pennsylvania State University
University Park, PA 16802, USA
E-mail: ncg2@psu.edu
L. Shen[†]
SHU-SolarE R&D Lab
Department of Physics
Shanghai University
Shanghai 200444, P.R. China
R. Dowdy, P. Froeter, Prof. X. Li
Department of Electrical and Computer Engineering
University of Illinois at Urbana-Champaign
Urbana, IL 61801, USA
Prof. R. G. Nuzzo
Department of Chemistry
University of Illinois at Urbana-Champaign
Urbana, IL 61801, USA
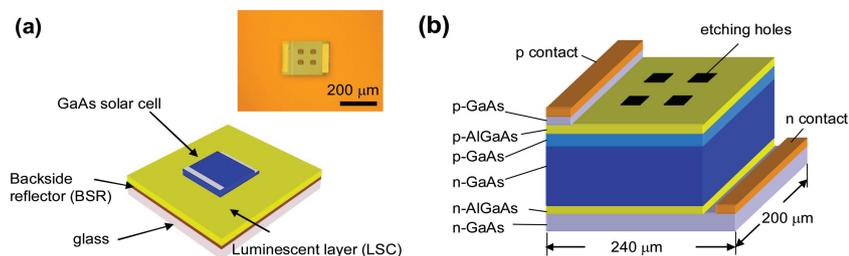[†]X.S. and L.S. contributed equally to this work.

COMMUNICATION

Figure 1. a) Schematic illustration of a GaAs μ-cell transfer printed onto a luminescent solar concentrator (LSC) layer, with a backside reflector (BSR) on the surface of a supporting glass substrate. Upper Inset: Optical microscope image of a GaAs μ-cell (200 μm × 240 μm) with four holes to facilitate epitaxial liftoff, and metallic Ohmic contacts, printed on an LSC substrate. b) Detailed structure of the cell, which includes a GaAs homojunction, AlGaAs window layers and contacting layers.

dye (4-(dicyanomethylene)-2-methyl-6-(p-dimethylaminostyryl)-4H-pyran) spin cast onto a glass substrate (1 mm thick) coated with either a specular back side reflector (BSR) of Ag (200 nm thick) or a diffuse BSR consisting of a dense layer of TiO_2 particles deposited on top of the Ag film. Although issues in long term reliability require further study, the polymer matrix materials and dyes used here are found in demanding commercial applications in lasers and integrated optics. Alternative LSC designs involve free-standing layers formed using a molding process. Other dye candidates are possible, such as Red305 and BA241.[14] The underlying physics and other general considerations reported here are independent of the choice of dye. The absorption and emission spectra of the polymer/DCM material appear in Figure S1. The DCM absorbs light with wavelengths between 300 nm and 600 nm; emission occurs between 550 nm and 750 nm. The quantum yield is 0.83 ± 0.04 for dye concentrations throughout the range explored here. Photons re-emitted at angles beyond the cone of total internal reflection are trapped in waveguided modes and may be absorbed at the backsides of the surface-mounted GaAs cells. The diffuse BSRs function as scattering plate concentrators, enabling up to a $2n^2$ intensity enhancement on the cell surface,[16] but do not efficiently sustain luminescent concentration since waveguided modes are not well supported in such systems.

Figure 2a shows a series of experiments designed to quantify the optical losses and collection efficiencies associated with each LSC configuration. Test structures involve specular and diffuse BSRs deposited on glass plates (1 mm thick), each with a 200 μm wide slit to enable passage of illuminating radiation from the backsides. Films of polymer/DCM (DCM concentration is 0.2 wt%) spin cast on such BSR layers form LSC layers with thicknesses of 150 μm (Experimental and simulation results from samples with various dye concentrations and layer thicknesses appear in Figure S4). Collimated emission from a blue light emitting diode (center wavelength 470 nm, linewidth 29 nm) directed through the slits in the BSRs generates luminescence in the LSC. A microscope objective coupled to a CCD spectrometer captures and records light escaping from the LSC at various distances, L, from the center of the slit. Figure 2b shows luminescent spectra measured at different L for both samples. As L increases, the amount of captured light decreases and the associated spectra exhibit a redshift. As shown in Figure 2c, the spectrally integrated luminescence intensity is

approximately one order of magnitude lower for the specular BSR than for the diffuse BSR, simply because out-coupled light in the specular case arises only from parasitic scattering of luminescent photons that are reabsorbed and re-emitted. Despite the overall difference in magnitude, the dependences of the intensities on L in both cases are remarkably similar for L > 0.8 mm. This observation is not simply due to the measurement geometry[10] and instead seems to imply that the outcoupling loss coefficient of inelastic scattering due to multiple reabsorption and re-emission events ultimately becomes comparable to that of elastic scattering from the diffuse BSR at large distances, despite the different physical nature of these processes. The spectral red-shift for the specular BSR case is larger than that for the diffuse BSR (Figure 2d) because measured light in the specular case involves a significant contribution from photons that have undergone multiple re-absorption and re-emission events (and consequently multiple opportunities for Stokes shifts), particularly at large L. Modeling these experiments by 3D ray-tracing simulations (solid lines in Figure 2c and 2d) quantitatively reproduces the observed trends. This experimental validation allows use of such models in isolating and understanding the effects of individual, underlying loss processes such as dye re-absorption and partial reflections at the BSR.

Various working LSC device configurations appear in **Figure 3**a; in all cases, the substrates have sizes of 25 mm by 37 mm. The LSC layers and GaAs μ-cells use designs described previously. A reference sample uses an undoped polymer layer (i.e., without DCM dye) on a specular BSR. Figures 3b and 3c display the measured and simulated external quantum efficiency (EQE) spectra obtained for each configuration. The EQE is defined as the ratio of the number of charge carriers collected by the solar cell to the number of photons at a given wavelength incident on the luminescent concentrator. As compared to the reference sample, the device on the LSC film with a specular BSR shows a large enhancement in EQE for wavelengths between 400 nm to 600 nm, as a result of luminescent concentration. At wavelengths beyond the absorption edge of the DCM (λ > 600 nm), the EQE curves of the reference cell and specular BSR LSC are nearly identical, as expected. The case of the diffuse BSR, on the other hand, shows a broadband, uniform increase in EQE in the spectral range from 400 nm to 900 nm, consistent with expectation for a scattering plate. Although this behavior leads to reductions in enhancements associated with luminescence at short wavelengths, the absorption over the entire solar spectrum is greater than that for an otherwise similar system that uses a specular BSR. The result is an improved short-circuit current (I_{sc}) under AM1.5G simulated solar illumination (0.1 W/cm²), as shown in Figure 3d. The values of I_{sc} for the specular (in blue) and diffuse (in black) BSR LSCs are larger than those of the reference device by factors of 1.57× and 1.71×, respectively.

As a means to exploit diffuse scattering at long wavelengths without sacrificing contributions from luminescence at short wavelengths, the diffuse BSR can be separated from the LSC
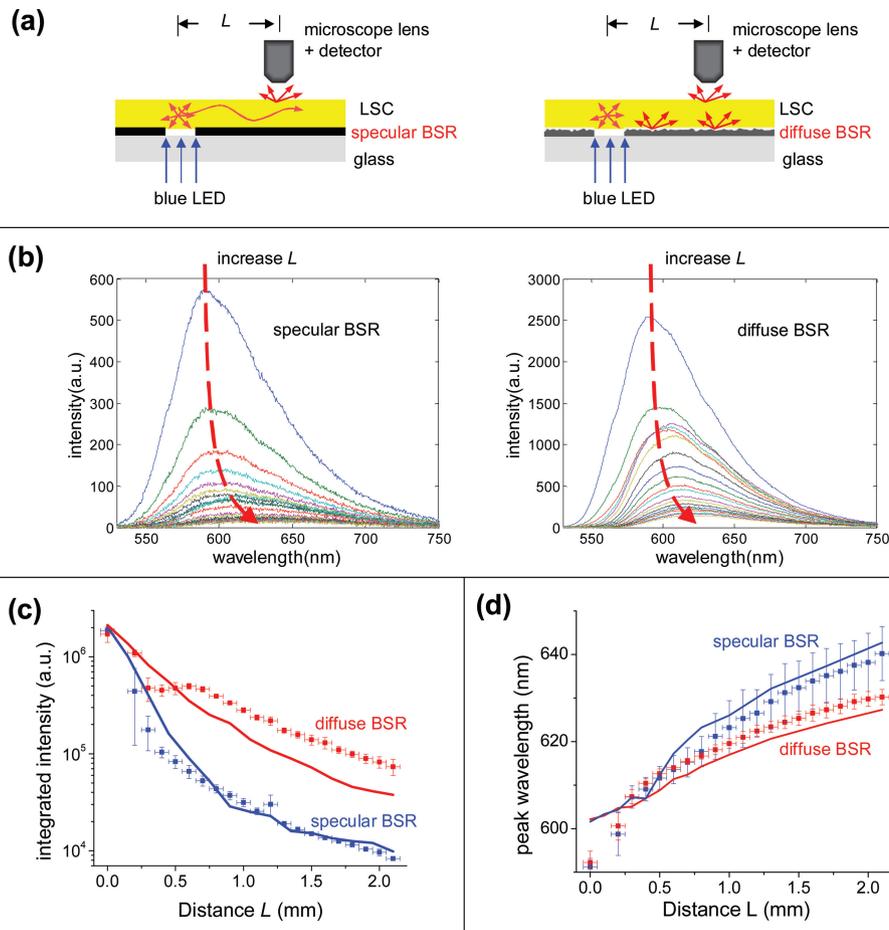
Materials
Views
www.MaterialsViews.com

ADVANCED
ENERGY
MATERIALS
www.advenergymat.de

COMMUNICATION

Figure 2. a) Experimental geometry for measuring optical transport in LSCs. Here, collimated light from a blue LED (centered at 470 nm) illuminates a slit (200 μm wide) in the BSR. Photons that escape from certain locations along the the top surface are captured by a microscope objective (numerical aperture = 0.95, working distance = 0.21 mm, 63× magnification) and recorded with a spectrometer. b) Measured luminescent spectra at different distances L for samples with specular and diffuse BSRs, indicating intensity decay and spectral red-shifts. To elucidate the decay in intensity and the shift in the peak position, we only show results for L from 0.2 mm to 2.2 mm. The curves for L = 0 are not shown, because the intensities are too high. c) Integrated luminescent intensity (from 540 nm to 750 nm) as a function of L. d) Peak wavelengths of luminescence as a function of L. The solid lines in these plots correspond to ray tracing simulation results.

layer by an air gap,[9,13] as shown at the bottom of Figure 3a. The presence of an air gap allows the structure to act as an efficient waveguide for photons that have a propagation angle larger than the critical angle for total internal reflection. The measured and calculated values of EQE appear in Figure 3b and 3c (in red), respectively. The results indicate that this configuration (in red) achieves a 2.21× increase in I_{sc} and a 2.32× increase in power conversion efficiency compared to the reference cell. The enhancement in this case exceeds that of the specular BSR case because of reductions in waveguide losses and increased absorption of incident light by the dye (via increased optical path length). Simulations capture these effects, although with some discrepancy at longer wavelengths where the calculated enhancement is lower than the experimentally measured values. From the standpoint of thermodynamics, the EQE for the case of the air-gap BSR design is expected (and predicted) to be lower in this long wavelength range than that of an otherwise similar LSC without the air gap due to decoupling of the BSR from the waveguide. This decoupling prevents the sorts

of trapping effects that can otherwise lead to increased optical pathlengths and consequent absorption.[16] That this is not the case in our data likely indicates that there are some areas in our structure where the LSC film touches the BSR directly, leading to an incomplete air gap.

The experimental and simulation results demonstrate the effectiveness of using a combination of luminescent concentration and scattering to improve the power output of bifacial GaAs μ-cells, when embedded directly in the surface of the LSC waveguide. The results also indicate, however, that additional improvement can be achieved by increasing the performance of the μ-cells. In particular, as shown in Figure S3, for designs used here, the quantum efficiency is significantly lower for light incident from the back sides of the cells than from their front sides, due largely to parasitic absorption in the n-GaAs contact layer. The simulations of Figure 3 account for this non-ideal behavior by disregarding the absorption in the contact layer, which represents nearly *half* of the light absorbed by the cell. Recovering this contribution can be achieved either directly by
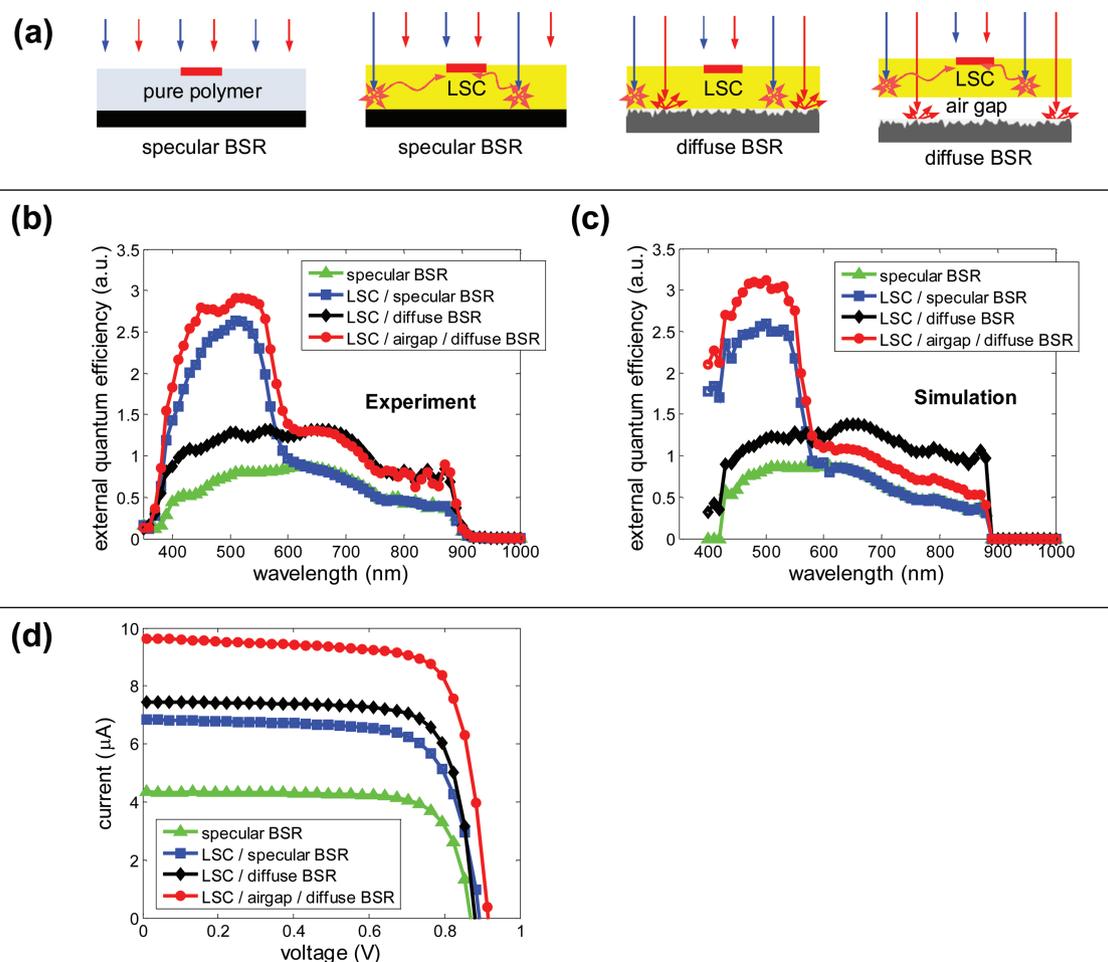
ADVANCED
ENERGY
MATERIALS
www.advenergymat.de

Materials
Views
www.MaterialsViews.com

Figure 3. a) Schematic illustrations of GaAs µ-cells embedded on the surfaces of different LSCs. b) Measured EQE spectra. c) Simulated EQE spectra. d) Measured current-voltage (*I–V*) characteristics under AM1.5G illumination. Substrates: PU/ specular BSR (green triangle), LSC/ specular BSR (blue square), LSC/ diffuse BSR (black diamond), LSC/ air gap/ diffuse BSR (red circle).

improving the quantum yield for back side illumination or by embedding cells with the existing designs at the bottom of the LSC layer so that all light is absorbed through the front side.

Figure 4a shows the total light absorbed by the cell as a function of illumination area, through a plot of the concentration ratio (CR) at 480 nm for the specular and diffuse LSC cases (without an air gap) of Figure 3. The CR is defined here as the ratio of the total number of photons absorbed by the GaAs cell (through both front and back surfaces) when incorporated in the LSC as compared to that absorbed by a free-standing cell at normal incidence. The CR thus represents the enhancement in EQE relative to the reference cell at $\lambda = 480$ nm for the ideal case where the internal quantum yield is the same for both front and back side illumination. The LSC with the specular BSR exhibits a CR that saturates slowly with increasing area, reaching a value of 7.1×, which is more than two times larger than that shown in Figure 3. In contrast, the LSC with the diffuse BSR saturates much more rapidly and reaches a reduced CR (2.7×), consistent with expected behavior of a scattering plate concentrator.

Figure 4b simulates the effects of dye concentration and LSC layer thickness on CR for an LSC with a specular BSR at

an incident wavelength of 480 nm. The results indicate that a maximum CR of 12.3× is possible at an optimum dye concentration (*c* = 0.12 wt%) and LSC thickness (*t* = 80 µm). This combination reflects a balance between several competing factors. On one hand, increases in dye concentration and LSC thickness increase the absorption. On the other, reductions in the concentration reduce self-absorption, and decreases in the thickness improve the probability of collecting luminescence within the waveguide (i.e. the cell occupies a larger portion of the optical phase space in the guide). To reveal the overall LSC performance, Figure 4c shows calculated flux gain (power increase factor compared to a bare cell without LSC) and cost per watt as a function of geometric gain (the ratio of the overall LSC area to the GaAs cell area) in an array integrated with an optimized LSC layer (*c* = 0.12 wt% and *t* = 80 µm), on a diffuse BSR separated by an air gap. With optimized designs, individual GaAs µ-cells can be expected to reach efficiencies of 20% and ideal bifacial performance;[1,3,20] we assume that the cost of the LSC and BSR is negligible compared to that of the cells. As the geometric gain increases, the flux gain and module cost per watt increase and decrease, respectively, due to the additional power generated through luminescent concentration. When
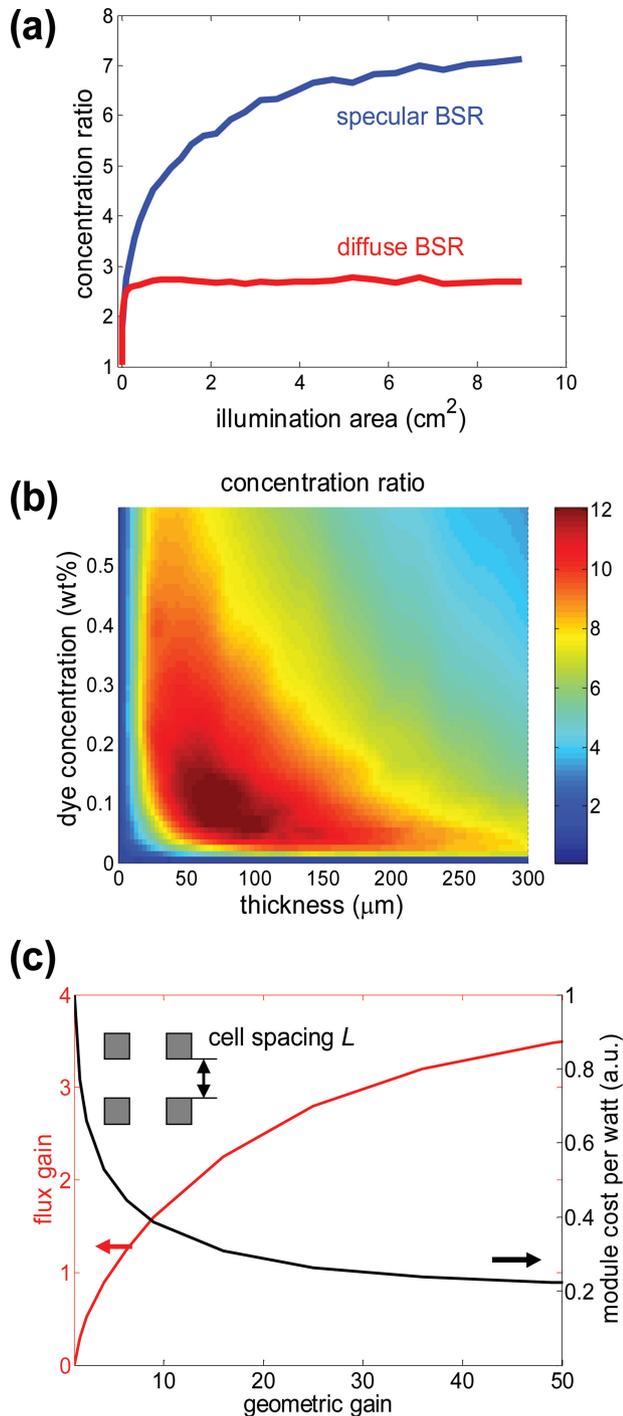
Figure 4. a) Calculated optical concentration ratios (for LSC based on specular and diffuse BSRs, dye concentration 0.2 wt% and thickness 150 µm) at 480 nm as a function of illumination area. b) Plot of calculated optical concentration ratio (CR) at 480 nm as a function of the LSC dye concentration and layer thickness, for LSC coated on a specular BSR. c) Calculated flux gain and cost per watt as a function of geometric gain, for GaAs µ-cell arrays in an optimized LSC configuration (i.e. diffuse BSR separated by an air gap).

the geometric gains are 4 and 9 (corresponding cell spacings are 0.2 mm and 0.4 mm), the flux gain can reach 0.9 and 1.6, leading to LSC collection efficiencies (flux gain/ geometric

gain) of 22% and 18%, respectively. Therefore, our optimized GaAs/LSC system can reach a better performance than our previously reported Si/LSC using the same dye/matrix materials,[6] and can, in fact, compete with LSC structures that incorporate much more advanced dye systems.[10]

In summary, we demonstrate that printing bifacial thin-film GaAs micro solar cells on LSC layers can more than double their output power under simulated solar illumination. Although conventional LSC designs and the approach presented here have many differences, both act to increase the effective areas of the cells. The epitaxial liftoff and transfer printing techniques represent methods for cell/LSC integration with potential for large scale module production. The considerations reported here are directly applicable to modules that incorporate large-scale arrays of cells, formed and manipulated using procedures described and demonstrated elsewhere.[1,5,6] The luminescent dyes provide solar energy conversion with reduced usage of III-V materials, with associated benefits in cost reduction. Careful experimental and theoretical studies suggest routes to further improvements, where an overall architecture that incorporates a free-standing LSC layer with a diffuse BSR delivers the highest photocurrent by combining the benefits of the waveguided luminescence and diffuse scattering. Significantly higher performance and greater cost reduction are predicted by implementing optimized LSC parameters, cell spacings and improved spectral response of the cell under back side illumination. Although the ultimate performance for a practical LSC system remains an open question, our approaches provide a glimpse of what is possible. The most significant opportunities for improving performance are in the development of advanced dyes. Additional avenues that can be explored, include, as examples, the shapes of the µ-cells and their positions within the LSC layer, advanced luminescent dye systems, with optimized concentration laterally and through the depth of the LSC.[14,21] The LSC design presented in this paper provides a guideline for broadband light management in highly efficient III-V semiconductor based solar cell modules.

Experimental Section

Fabrication and integration of GaAs solar micro cells: The GaAs solar cell structure was grown on a GaAs substrate by metal-organic chemical vapor deposition (MOCVD). The n-type GaAs and p-type GaAs layers were achieved by Si doping and Zn doping, respectively. The detailed structure (from bottom to top) involves the GaAs substrate, a 1 µm $Al_{0.95}Ga_{0.05}As$ sacrificial layer, a 300 nm n-GaAs bottom contact ($n = 5 \times 10^{18}$ cm^{-3}), a 50 nm n-$Al_{0.4}Ga_{0.6}As$ back surface field (BSF) layer ($n = 4 \times 10^{17}$ cm^{-3}), a 2 µm n-GaAs base ($n = 3 \times 10^{17}$ cm^{-3}), a 100 nm p-GaAs emitter ($p = 2 \times 10^{18}$ cm^{-3}), a 30 nm p-$Al_{0.4}Ga_{0.6}As$ window layer ($p = 2 \times 10^{18}$ cm^{-3}) and a 200 nm p-GaAs top contact ($p = 1 \times 10^{19}$ cm^{-3}). Ohmic contacts on the n-GaAs and p-GaAs were formed by evaporating 5 nm Pd/ 35 nm Ge/ 80 nm Au and 10 nm Cr/ 100 nm Au, followed by annealing at 175 °C for 1 hour in N$_2$ ambient. After the $Al_{0.95}Ga_{0.05}As$ sacrificial layer was etched in mixed concentrated HF (49%) and deionized water in a ratio of 1:20 (by volume), the GaAs solar cells were lifted off and transferred onto other substrates by transfer printing with a flat polydimethylsiloxane (PDMS) (Sylgard 184, Dow Corning) stamp, as previously reported.[1] The resulting GaAs solar cells appear in Figures 1b and 1c.

Fabrication of backside reflectors (BSRs): The specular BSR was prepared by evaporating 15 nm Ti/ 200 nm Ag on a 1 mm thick glass slide. Spin casting a mixture of 3 wt% TiO$_2$ powder and 2 wt% polyacrylic

COMMUNICATION

acid (Sigma-Aldrich) in isopropanol on the Ag coated glass, yielded a diffuse BSR. The reflection spectra were collected with an integrating sphere in a UV-vis spectrometer (Cary 5G, Varian). See Figure S2.

Fabrication of the luminescent solar concentrator (LSC): The DCM dye (Exciton Inc.) was mixed into the UV curable polymer (NOA61, Norland Products Inc.).[6] The resulting solution was spin cast onto the BSR and cured under UV illumination, to yield the LSC substrates. The free standing LSC was formed by curing the polymer/DCM in a mold made of PDMS. All LSC substrates shown in Figure 4a had dimensions of 25 mm × 37 mm, with GaAs μ-cells printed in the center. The photoluminescence quantum yields for the DCM-doped polymer films were measured using in an integrating sphere following standard procedures.[22]

Device Characterization: The current-voltage relation was measured by a Keithley 2400 source meter under illumination provided by a 1200 W Newport solar simulator passing through a standard Air Mass 1.5 Global (AM1.5G) filter. External quantum efficiency (EQE) spectra were collected using a Halogen lamp coupled to a Jarrell-Ash Monospec 27 monochromater scanning from 350 nm to 1000 nm, with a beam size of about 4 cm by 4 cm.

Ray tracing model: Non-sequential ray tracing simulations were carried out using the commercially available software package, Zemax,[23] accounting for all Fresnel reflections using measured and literature optical constant dispersions for NOA61, Ag, and GaAs. (Alternatively, a custom coded ray-tracing package using same parameters produced similar results.) The measured absorption coefficient, photoluminescence spectrum and quantum yield of 0.2 wt% DCM-doped NOA61 were included as well as the diffuse reflectance measured for the diffuse BSR in Figure S2. Light absorption was spatially resolved within 100 nm slices inside the GaAs μ-cells. Absorption in the bottom 0.3 μm thickness of the cells does not generate any photocurrent whereas the IQE for light absorbed in the top 1.7 μm was calculated to be consistent with the front illuminated EQE of the bare cell in Figure S3a. In simulations for the slit experiments of Figure 2, multiple reabsorption and re-emission was considered explicitly, with secondary photons emitted within the photoluminescence spectrum at wavelengths equal to or larger than the absorbed photons. The microscope objective was modeled as a perfectly absorbing, 100 μm × 100 μm detector spaced from the LSC surface by the objective working distance and with an angular acceptance corresponding to the numerical aperture. For simulations in Figures 3c and 4b, a GaAs μ-cell (200 μm × 240 μm × 2 μm) was embedded on the surface of a planar LSC layer (3 cm × 3 cm), with periodic boundary conditions used to simulate the cell array in Figure 4c.

Supporting Information

Supporting Information is available from the Wiley Online Library or from the author.

Acknowledgements

[1] J. Yoon, S. Jo, I. S. Chun, I. Jung, H. Kim, M. Meitl, E. Menard, X. Li, J. J. Coleman, U. Paik, J. A. Rogers, *Nature* **2010**, *465*, 329.

[2] X. Y. Lee, A. K. Verma, C. Q. Wu, M. Goertemiller, E. Yablonovitch, *Proc. 25th IEEE Photovoltaic Spec. Conf.* **1996**, 53.

[3] M. A. Green, K. Emery, Y. Hishikawa, W. Warta, E. D. Dunlop, *Prog. Photovolt: Res. Appl.* **2012**, *20*, 606.

[4] http://www.semprius.com/pdf/press_releases/press_release_19.pdf (accessed March 2013).

[5] J. Yoon, A. J. Baca, S. Park, P. Elvikis, J. B. Geddes, L. Li, R. H. Kim, J. Xiao, S. Wang, T. Kim, M. J. Motala, B. Y. Ahn, E. B. Duoss, J. A. Lewis, R. G. Nuzzo, P. M. Ferreira, Y. Huang, A. Rockett, J. A. Rogers, *Nat. Mater.* **2008**, *7*, 907.

[6] J. Yoon, L. Li, A. V. Semichaevsky, J. H. Ryu, H. T. Johnson, R. G. Nuzzo, J. A. Rogers, *Nat. Comm.* **2011**, *2*, 343.

[7] W. H. Weber, J. Lambe, *Appl. Opt.* **1976**, *15*, 2299.

[8] A. Goetzberger, W. Greubel, *Appl. Phys.* **1977**, *14*, 123.

[9] L. H. Slooff, E. E. Bende, A. R. Burgers, T. Budel, M. Pravettoni, R. P. Kenny, E. D. Dunlop, A. Buchtemann, *Phys. Status Solidi RRL* **2008**, *2*, 257.

[10] M. J. Currie, J. K. Mapel, T. D. Heidel, S. Goffri, M. A. Baldo, *Science* **2008**, *321*, 226.

[11] W. van Sark, K. W. J. Barnham, L. H. Slooff, A. J. Chatten, A. Buchtemann, A. Meyer, S. J. McCormack, R. Koole, D. J. Farrell, R. Bose, E. E. Bende, A. R. Burgers, T. Budel, J. Quilitz, M. Kennedy, T. Meyer, C. Donega, A. Meijerink, D. Vanmaekelbergh, *Opt. Express* **2008**, *16*, 21773.

[12] N. C. Giebink, G. P. Wiederrecht, M. R. Wasielewski, *Nat. Photonics* **2011**, *5*, 694.

[13] L. Desmet, A. J. M. Ras, D. K. G. de Boer, M. G. Debije, *Opt. Lett.* **2012**, *37*, 3087.

[14] M. G. Debije, P. P. C. Verbunt, *Adv. Energy Mater.* **2012**, *2*, 12.

[15] G. Smestad, H. Ries, R. Winston, E. Yablonovitch, *Sol. Energy Mat.* **1990**, *21*, 99.

[16] E. Yablonovitch, G. D. Cody, *IEEE Trans. Elect. Dev.* **1982**, *ED–29*, 300.

[17] E. Yablonovitch, *J. Opt. Soc. Am.* **1980**, *70*, 1362.

[18] D. J. Farrell, M. Yoshida, *Prog. Photovolt: Res. Appl.* **2012**, *20*, 93.

[19] A. Carlson, A. M. Bowen, Y. Huang, R. G. Nuzzo, J. A. Rogers, *Adv. Mater.* **2012**, *24*, 5284.

[20] J. J. Schermer, G. J. Bauhuis, P. Mulder, E. J. Haverkamp, J. van Deelen, A. T. J. van Niftrik, P. K. Larsen, *Thin Solid Films* **2006**, *511–512*, 645.

[21] C. Wurth, K. Hoffmann, T. Behnke, M. Ohnesorge, U. Resch-Genger, *J. Fluoresc.* **2011**, *21*, 953.

[22] J. N. Demas, G. A. Crosby, *J. Phys. Chem.* **1971**, *75*, 991.

[23] http://www.radiantzemax.com (accessed March 2012).

[24] Y. Liu, Y. Sun, A. Rockett, *Sol. Energ. Mat. Sol. Cells* **2012**, *98*, 124.